Superconductivity at 253 K in lanthanum–yttrium ternary hydrides

Dmitrii V. Semenok [1,†], Ivan A. Troyan [2,†], Anna G. Ivanova [2,†], Alexander G. Kvashnin [1,*,†], Ivan A. Kruglov [3,4], Michael Hanfland [5], Andrey V. Sadakov [6], Oleg A. Sobolevskiy [6], Kirill S. Pervakov [6], Igor S. Lyubutin [2], Konstantin V. Glazyrin [7], Nico Giordano [7], Denis N. Karimov [2], Alexander L. Vasiliev [2,4], Ryosuke Akashi [8], Vladimir M. Pudalov [6,9], Artem R. Oganov [1,*]

[1] Skolkovo Institute of Science and Technology, Skolkovo Innovation Center, 3 Nobel Street, Moscow 121205, Russia
[2] Shubnikov Institute of Crystallography, Federal Scientific Research Center Crystallography and Photonics, Russian Academy of Sciences, 59 Leninsky Prospekt, Moscow 119333, Russia
[3] Dukhov Research Institute of Automatics (VNIIA), Moscow 127055, Russia
[4] Moscow Institute of Physics and Technology, 9 Institutsky Lane, Dolgoprudny 141700, Russia
[5] ID15B High Pressure Diffraction Beamline, ESRF, BP220, Grenoble 38043, France
[6] P. N. Lebedev Physical Institute, Russian Academy of Sciences, Moscow 119991, Russia
[7] Deutsches Elektronen-Synchrotron, D-22607 Hamburg, Germany
[8] University of Tokyo, 7-3-1 Hongo, Bunkyo, Tokyo 113-8654, Japan
[9] National Research University Higher School of Economics, Moscow 101000, Russia

Here we report the high-pressure synthesis of a series of lanthanum–yttrium ternary hydrides obtained at pressures of 170–196 GPa via the laser heating of $P6_3/mmc$ La–Y alloys with ammonia borane. As a result, we discovered several novel compounds: cubic hexahydride (La,Y)H_6 and decahydrides (La,Y)H_{10} with a maximum critical temperature $T_C \sim 253$ K and an extrapolated upper critical magnetic field $B_{C2}(0)$ of up to 135 T at 183 GPa. The current–voltage measurements show that the critical current density J_C in (La,Y)H_{10} is 12–27.7 kA/mm^2 at 4.2 K, which is comparable with that of commercial superconducting wires such as NbTi and Nb_3Sn. (La,Y)H_6 and (La,Y)H_{10} are among the first examples of ternary high-T_C superconducting hydrides. Our experiments show that part of metal atoms in the structures of recently discovered $Im\bar{3}m$-YH_6 and $Fm\bar{3}m$-LaH_{10} can be replaced with lanthanum (~70%) and yttrium (~25%), respectively, with the formation of unique ternary superhydrides containing metal-encapsulated cages La@H_{24} and Y@H_{32}, which are specific for $Im\bar{3}m$-LaH_6 and $Fm\bar{3}m$-YH_{10}. This work demonstrates that hydrides, unstable in pure form such as LaH_6 and YH_{10}, may nevertheless be stabilized at relatively low pressures in solid solutions with superhydrides having the desired structure.

Keywords: Superconductivity; Hydrides; USPEX; SCDFT; High pressure

* Corresponding authors.
E-mail addresses: Semenok, D.V. (dmitrii.semenok@skoltech.ru), Kvashnin, A.G. (A.Kvashnin@skoltech.ru).
† These authors contributed equally to this work.

 https://doi.org/10.1016/j.mattod.2021.03.025

Introduction

Metallic hydrogen is expected to display remarkable superconducting properties stemming from its high Debye temperature and strong electron–phonon coupling [1–4]. Theoretical calculations [5–7] show that metallization of hydrogen takes place only at extremely high pressures above 450 GPa, which have not been technically achievable for a long time. The renaissance of hydride superconductivity began in 2004 when Ashcroft [1] suggested that hydrogen-dominant metallic alloys may have high critical superconducting temperatures at much lower pressures. This scenario was realized in sulfur hydride [8] and in lanthanum hydride [9,10] at pressures below 200 GPa. Moreover, near-room-temperature superconducting transition (at 288 K), which is believed to be described within the conventional phonon-mediated mechanism of coupling, has been reported lately in carbonaceous sulfur hydride [11] at about 270 GPa. Recent series of successful experimental syntheses of high-temperature superconductors LaH_{10}, YH_6, and YH_9 [9,10,12–16] containing the metallic H sublattice motivated us to attempt to raise the critical temperature of the La – H and Y – H systems without increasing the pressure by combining the elements into ternary La–Y hydrides.

Distinctive features of hydrides are the transparency of the mechanism of their superconductivity, simplicity of calculations of the main parameters of the superconducting state, and close agreement between predictions and experiments. Several binary hydrides of yttrium and lanthanum have been discovered in the last few years (Supporting Information Table S6). In 2015, in the work of Li et al. [17], $Im\bar{3}m$-YH_6 was predicted to be stable at pressures over 110 GPa, with the superconducting transition temperature, found via the numerical solution of the Migdal–Eliashberg equations, in the range of 251–264 K at 120 GPa. Recently, we have synthesized YH_6 and shown [13] that it has a much lower critical temperature, about 224 K at 166 GPa. In 2017, in a detailed theoretical study of yttrium and lanthanum hydrides, Liu et al. [18] found that lanthanum hexahydride $Im\bar{3}m$-LaH_6 (isostructural to YH_6), lower-symmetry $R\bar{3}m$-LaH_6, and $Fm\bar{3}m$-YH_{10} are thermodynamically unstable and lie above the convex hull, which is a surface of the lowest free energy as a function of chemical composition, at pressures of at least up to 200 GPa. We wondered whether these unstable compounds could be stabilized in ternary alloys with a similar structure.

Theoretical studies of several ternary hydride systems such as Ca–Y–H [19], Ca–Mg–H [20], and Li–Mg–H [21] carried out in recent years indicated a possibility of increasing the superconducting critical temperature in comparison with binary hydrides. However, ternary La–Y hydrides have not been systematically examined yet. Some hints of their promising superconducting properties have been made: using the neural network [22], we have found that La–Y–H is one of the most encouraging systems to achieve room-temperature superconductivity. At the same time, Kostrzewa et al. [23], analyzing the dependence of the logarithmically averaged frequency ω_{log} on the mass of atoms, have predicted that the La–Y–H ternary hydrides may have T_C up to 274 K at 190 GPa.

In this work, we theoretically and experimentally investigated the superconducting properties of cubic hexahydrides $La_xY_{1-x}H_6$ and decahydrides $La_xY_{1-x}H_{10}$ obtained via laser heating of yttrium–lanthanum alloys with ammonia borane (AB, NH_3BH_3) used as a hydrogen source. Samples were compressed to 170–196 GPa in diamond anvil cells and heated by a series of laser pulses of 100–400 milliseconds duration. The superconducting properties of yttrium–lanthanum polyhydrides were investigated using the electrical transport measurements in different current modes and external magnetic fields. Ab initio calculations were used to unravel the composition and structure of the obtained compounds, as well as details of the mechanism of their superconductivity.

Results and discussion

Structure prediction

The study of yttrium hexahydride, synthesized at high pressures [13], has demonstrated that its critical temperature of superconductivity is significantly lower than theoretically predicted [24]. Is it possible to improve the parameters of the superconducting state by introducing another metal into the Y – H system? We noticed that lanthanum could form $Im\bar{3}m$-LaH_6, which lies only slightly above thermodynamic stability (i.e. the convex hull, Fig. 1) at 150–200 GPa [18]. This cubic LaH_6 can be, at least kinetically, stabilized by an isostructural environment of YH_6, which is of great interest in terms of high-temperature superconductivity because of the structural analogy with yttrium hexahydride.

Using evolutionary algorithm USPEX [25–27], we searched for thermodynamically stable phases in the La – Y – H system (Fig. 1) and found that at 200 GPa and 0 K none of the ternary hydrides are on the 3D convex hull except $LaYH_{20}$. Below in this paragraph we denote the symmetry of compounds without distinguishing Y and La. Surprisingly, $P6_3/mmc$-$LaYH_{20}$ is stable at 0 K (Fig. 1a), whereas the cubic modification $Fm\bar{3}m$-$LaYH_{20}$ is 50 meV/atom above the convex hull. An increase in temperature to 1000 K leads to the stabilization of tetragonal $I4/mmm$-La_2YH_{12} and cubic hexahydrides La_4YH_{30} and $LaYH_{12}$. These phases are metastable at 0 K, with the distances from the convex hull equal to 82, 38, and 53 meV/atom, respectively. Moreover, La_4YH_{50}, which belongs to the $La_{1-x}Y_xH_{10}$ structure type ($x = 0.2$), becomes stable at 1000 K. These structures can be considered as solid solutions of YH_{10} in $Fm\bar{3}m$-LaH_{10}. Other phases that belong to the $La_{1-x}Y_xH_{10}$ group (La_3YH_{40}, La_2YH_{30}, and LaY_4H_{50}) are 5, 8, and 13 meV/atom above the convex hull at 1000 K (Fig. 1b). Further increase in temperature to 1500 K leads to the stabilization of LaY_4H_{50} and La_2YH_{18} (Fig. 1c), whereas higher temperature of 2000 K stabilizes the La_2YH_{30} phase (Fig. 1d). Above 1800 K, $Fm\bar{3}m$-$LaYH_{20}$ also becomes stable (at 2000 K, $P6_3/mmc$-$LaYH_{20}$ is 5 meV/atom above the convex hull).

Recently, Song et al. [28] conducted a more detailed analysis of the thermodynamic stability of $LaYH_{12}$ clathrate structures, proposing several new structures in the La–Y–H system: semimetallic nonsuperconducting $R\bar{3}c$-$LaYH_{12}$, stable at 100–130 GPa, and $Cmmm$-$LaYH_{12}$, stable at 140–300 GPa, with relatively low $T_C = 140$ K at 200 GPa. At 0 K and 200 GPa, phase $R\bar{3}c$ (with 78 atoms per unit cell) has the enthalpy of formation which is 24 meV/atom lower than that of $Pm\bar{3}m$-$LaYH_{12}$ studied in this work. The enthalpy of formation of another polymorphic

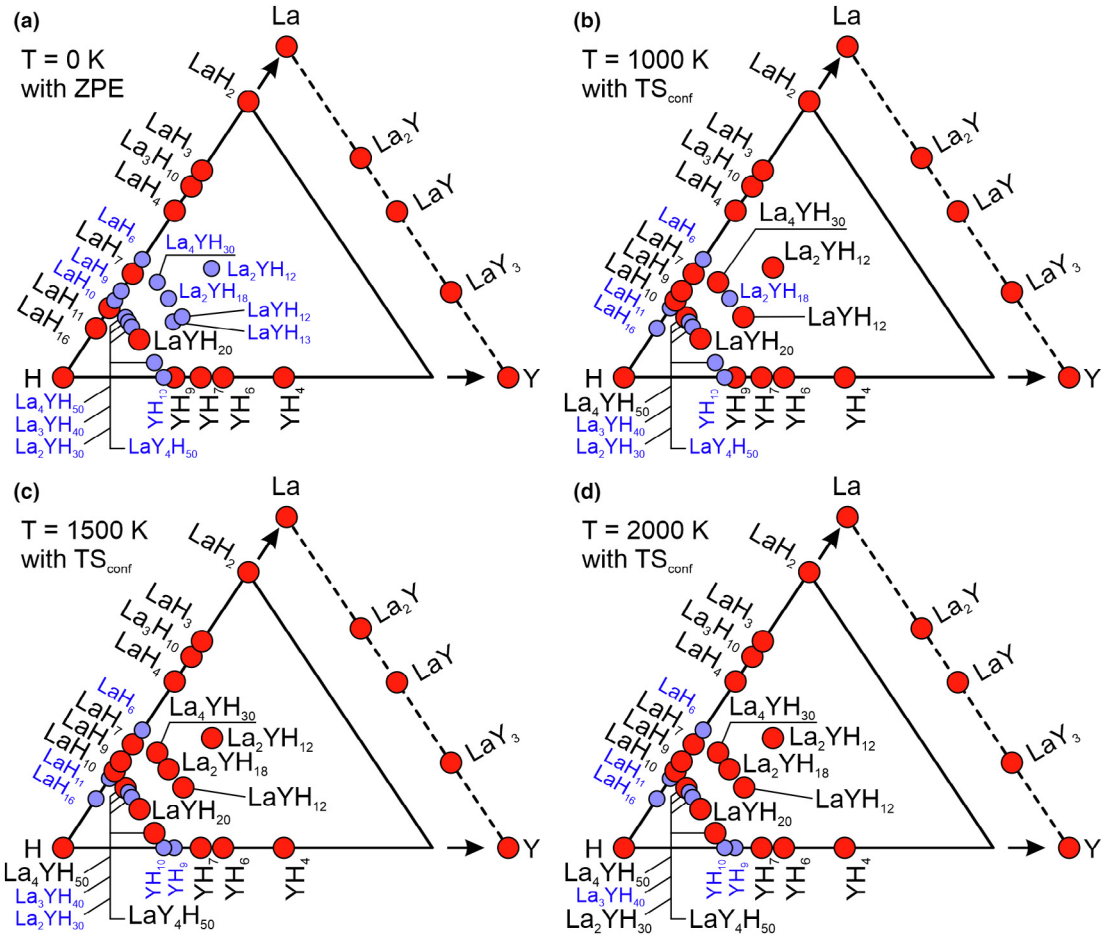

FIGURE 1

Ternary convex hulls of the La–Y–H system at a pressure of 200 GPa and temperatures of (a) 0 K, (b) 1000 K, (c) 1500 K, and (d) 2000 K, calculated with a contribution of the configurational entropy TS_{conf} and the zero-point energy (ZPE). The invisible *Z* axis, perpendicular to the plane of the figure, corresponds to the enthalpy of formation. Stable and metastable phases are shown in red and blue, respectively.

modification proposed by Song et al. [29], *Cmmm*-$LaYH_{12}$ (28 atoms per unit cell), is 6 meV/atom lower than that of phase $Pm\bar{3}m$. Calculations at temperatures of 1500–2000 K in the harmonic approximation show the same order of the structures by the energy. It is important that all mentioned polymorphic modifications of $LaYH_{12}$ have very similar X-ray diffraction patterns. Moreover, as we show below, in all the experimentally studied compounds, the critical temperature is significantly higher than 200 K and may not be attributed to the $R\bar{3}c$ or *Cmmm* modifications of $LaYH_{12}$.

Phonon calculations show that only La_2YH_{18} is dynamically stable within the harmonic approximation (Supporting Information Figs. S38–S40). However, an anharmonicity induced all investigated La–Y hydrides become dynamically stable, although in a number of cases (LaH_6, $LaYH_{20}$) their crystal structure is distorted (Supporting Information Figs. S41–S43). Under the entire range of studied pressure–temperature conditions, pure $Im\bar{3}m$-LaH_6 and $Fm\bar{3}m$-YH_{10} were thermodynamically unstable.

High-pressure synthesis

To synthesize promising superconducting ternary yttrium–lanthanum hydrides, we prepared a series of La–Y alloys: La_4Y, La_3Y, La_2Y, LaY, and LaY_4. The yttrium (>99.99%) and lanthanum (>99.99%) metal pieces were mixed with the selected molar ratio and a total weight of 1 g, pressurized, and melted several times in an argon arc while the sample was rotated to homogenize the melt. Subsequent X-ray and electron diffraction, X-ray fluorescence (XRF), and energy-dispersive X-ray (EDX) analyses showed that the hexagonal phase $P6_3/mmc$-La_xY_{1-x} is the main product of the alloying (Supporting Information Figs. S3–S5, S10–S11, S14–S15).

For loading high-pressure diamond anvil cells (DACs), we took the material from a homogeneous region of the alloy surface with the desired La:Y ratio determined by the EDX and XRF. To measure the synchrotron X-ray diffraction (XRD) and the critical temperature of superconductivity of synthesized lanthanum–yttrium hydrides, we used seven DACs (M1-2, M2_S, SL1, SL1_S, SL3, and SL3_S) with a 50 μm culet beveled to 300 μm at 8.5°, equipped with four ~200 nm thick Ta electrodes with ~80 nm gold plating (Fig. 3c) that were sputtered onto the piston diamond. Ammonia borane was used as a hydrogen source, following the technique that has shown good results in previous studies [13,29–33]. The detailed description of the DACs is presented in Supporting Information.

In five out of seven diamond anvil cells prepared for the XRD studies, the main observed phase was $Fm\bar{3}m$-$(La,Y)H_{10}$ (Fig. 2a,b,

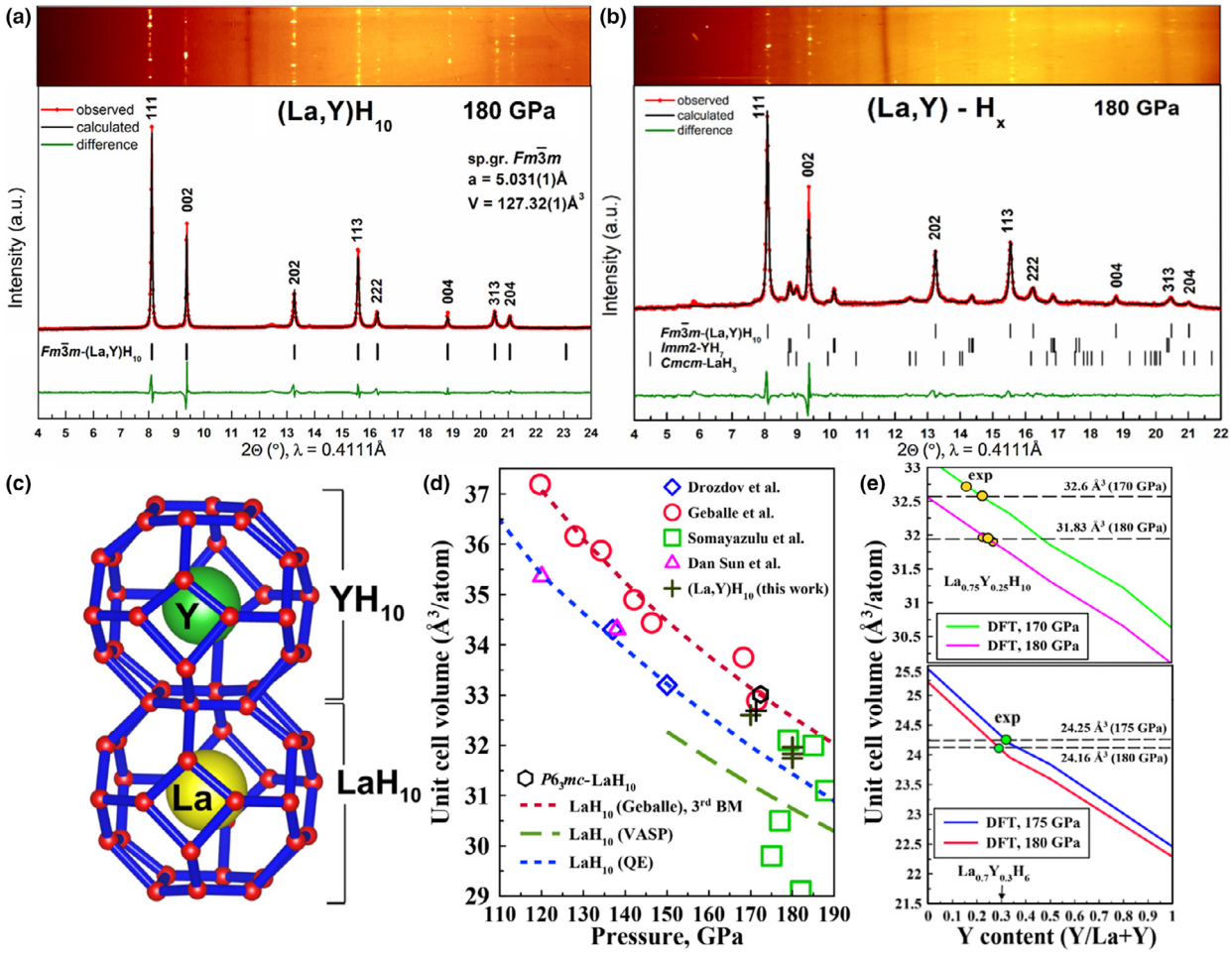

FIGURE 2

X-ray diffraction of La-Y hydrides. Experimental diffraction patterns and Le Bail refinements of the crystal unit cell parameters of (a) $Fm\bar{3}m$-(La,Y)H_{10} (DAC SL1**)** and (b) *Imm*2-YH_7 and *Cmcm*-LaH_3 (DAC M1**)**. The experimental data, fit, and residues are shown by red, black, and green lines, respectively. (c) Fragment of crystal structure of (La,Y)H_{10} where Y and La are neighbors (for illustrative purposes). (d) Pressure–unit cell volume diagram for *fcc* LaH_{10}: circles, squares, rhombuses, triangles, and crosses show the experimental data, lines depict the theoretical calculations. (e) Estimates of the Y content in (La,Y)H_{10} and (La,Y)H_6 obtained using the experimental unit cell volumes.

Supporting Information Figs. S18–S21) with a unit cell volume of ~31.8 Å^3 at 180 GPa, which is about 0.5–0.83 Å^3/f.u. lower than the volume of $Fm\bar{3}m$-LaH_{10} found by Geballe et al. [12] (Fig. 2d, Table 1 and Supporting Information Table S5). The decrease in the unit cell volume is due to the replacement of large La atoms with Y, which have a smaller size. In the discovered ternary cubic La–Y polyhydride, the substitution of the La atoms with Y resulted in the formation of the Y@H_{32} fragments with a locally distorted H-cage specific to $Fm\bar{3}m$-YH_{10} (Fig. 2c) [18].

There are large differences in the parameters of the unit cell of LaH_{10} reported by different research groups [9,10,12,18,34]. In the first experiment by Geballe et al. [12], the unit cell volume of LaH_{10} at about 170 GPa was over 33 Å^3, which is significantly larger than 31.2 Å^3 calculated theoretically using VASP (Fig. 1d, red circles). This prompted the authors of Ref. [12] to attribute the undefined stoichiometry LaH_{9-12} to the discovered compound [12].

In the subsequent studies by Drozdov et al. [10] and Sun et al. [35], the experimental cell volume values of the synthesized LaH_{10} (V = 33.2 Å^3 at 150 GPa) are smaller by about 1.2 Å^3/f.u. than those observed by Geballe et al. [12] (Fig. 2d). However, they are larger than those predicted using VASP [36–39], and are in close agreement with the equations of state (EoS) calculated using the Quantum ESPRESSO [40,41] pseudopotentials (Fig. 2d, "QE", blue line). In both cases the Perdew–Burke–Ernzerhof functional [42] (generalized gradient approximation) was used. The experimental data of Sun et al. [35] were obtained in the low pressure range of 120–150 GPa, where distortion of the ideal cubic structure of $Fm\bar{3}m$-LaH_{10} ($\rightarrow C2/m$) occurs [35] and, at the same time, there is a possibility of losing some hydrogen from the crystal structure.

Given the substantial uncertainty in both theoretical (Supporting Information Table S4) and experimental equations of states, and taking into account that the substitution of La with Y in LaH_{10} should lead to a decrease in the unit cell volume, we performed an additional experiment with pure La compressed with AB in DAC SL3_S at 171 GPa. After the laser heating of the sample, we detected the formation of $Fm\bar{3}m$-LaH_{10} with the unit cell volume of 32.82 Å^3 (Supporting Information Fig. S22) and an impurity hexagonal ($P6_3mc$) LaH_{10} phase with the unit cell volume of 33.05 Å^3 (Supporting Information Fig. S23), which was also detected in previous experiments [10]. Thus, taking into

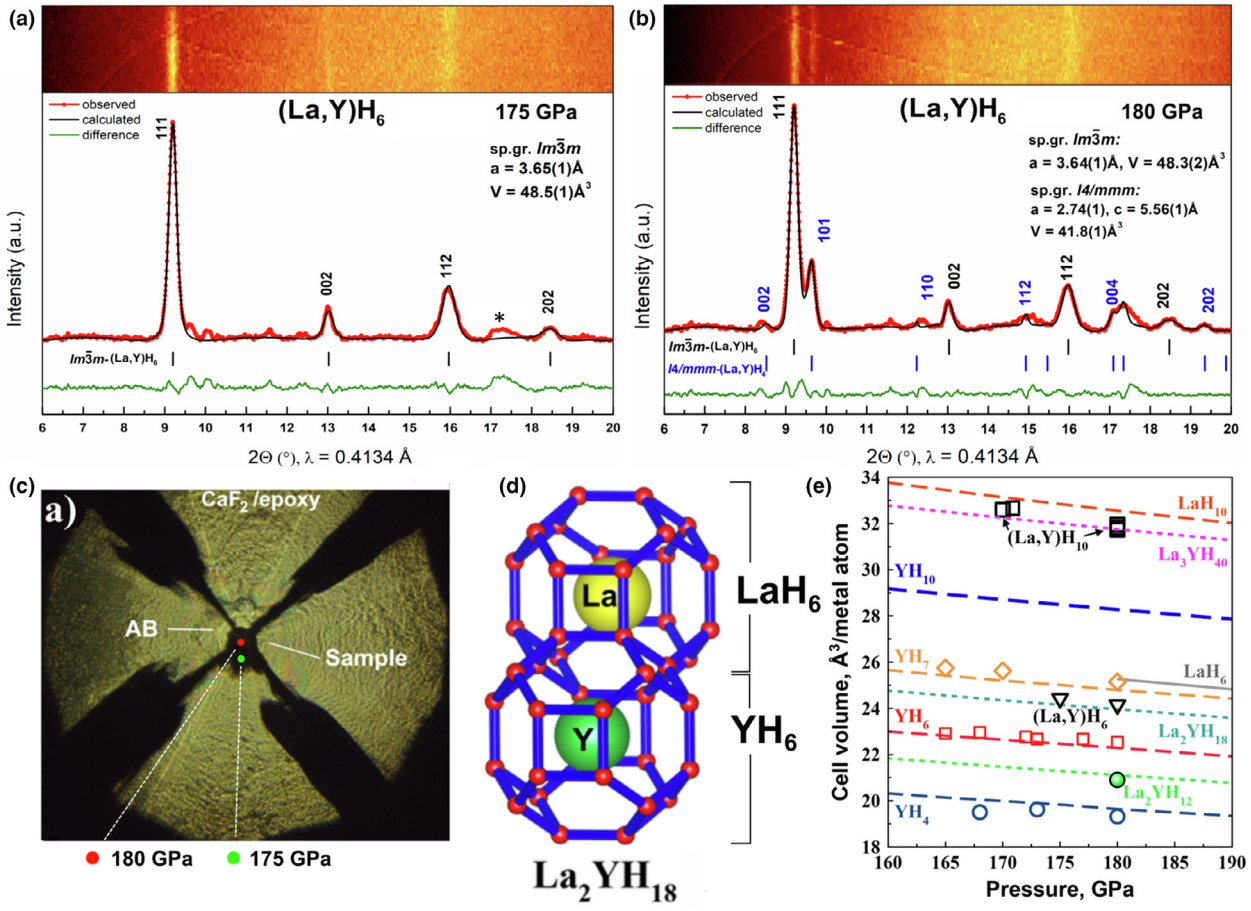

FIGURE 3

X-ray diffraction study of the La–Y hydrides in DAC M2_S. (a, b) Experimental diffraction patterns and Le Bail refinements of the cell parameters of $Im\bar{3}m$-(La,Y)H_6 and tetragonal *I4/mmm*-(La,Y)H_4 at 175 and 180 GPa. Experimental data, fit, and residues are shown in red, black, and green, respectively. (c) Optical microscopy of the loaded DAC: sample, NH_3BH_3 medium, and four Ta/Au electrodes. (d) Fragment of the crystal structure of (La,Y)H_6 where Y and La are neighbors (for illustrative purposes). (e) Pressure–unit cell volume diagram of the studied La–Y–H phases.

TABLE 1

Experimental lattice parameters and unit cell volumes of $Fm\bar{3}m$-(La,Y)H_{10} ($Z = 4$), $Im\bar{3}m$-(La,Y)H_6, $Fm\bar{3}m$-LaH_{10} ($Z = 4$) and $P6_3mc$-LaH_{10} ($Z = 2$).

DAC	Pressure, GPa	*a*, Å	*V*, Å^3
***Fm*$\bar{3}$*m*-(La,Y)H_{10}**			
M1	180	5.038(1)	127.86(2)
M2	180	5.026(1)	126.98(2)
SL1	180	5.031(1)	127.32(1)
SL3	170	5.071(1)	130.40(1)
***Im*$\bar{3}$*m*-(La,Y)H_6**			
M2_S	175	3.65(1)	24.26
M2_S	180	3.64(1)	24.16
***Fm*$\bar{3}$*m*-LaH_{10}**			
SL3_S	171	5.08(1)	131.3(1)
	171	5.07(1)	130.8(1)
***P*6_3*mc*-LaH_{10}**			
SL3_S	171	3.60(1) 5.88(1)	66.1(1)

account that our experimental result for $V(LaH_{10})$ is close to the data of Ref. [12], we chose the 3rd order Birch–Murnaghan interpolation [43,44] of the experimental EoS found by Geballe et al. [12] as a reference (Fig. 2d, red dotted line). Using this EoS, we determined the composition of synthesized (La,Y)H_{10} as La_3YH_{40} or $La_{0.75}Y_{0.25}H_{10}$ (Fig. 2e), in which the La:Y ratio is close to that

of the loaded sample in DACs M2, SL1, and SL1_S. Indeed, the results of the X-ray structure analysis show that the cleanest samples of (La,Y)H_{10} were obtained in DACs SL1, SL1_S, and M2, whereas in DACs M1 (loaded with LaY) and SL3 (loaded with LaY_4) we detected a notable amount of previously described [13] impurities: pseudocubic *Imm*2-YH_7 and, probably, *Cmcm*-LaH_3 (Supporting Information Figs. S19–S20), formed as decomposition products: (La,Y)H_{10} → LaH_3 + YH_7.

For DAC M2_S, loaded with La_2Y/AB, the X-ray diffraction patterns (Fig. 3a,b) were identical to the one previously observed for $Im\bar{3}m$-YH_6 [13]. However, the obtained unit cell volumes of 48.5–48.3 Å^3 (Z = 2, 175–180 GPa) are in sharp contrast with that of YH_6 (<46 Å^3, Fig. 3e) in the same pressure interval. Given that the volume of hypothetical $Im\bar{3}m$-LaH_6 is above 50 Å^3 (Z = 2), the resulting product (La,Y)H_6 can be described as La_2YH_{18} (more accurately, $La_{0.7}Y_{0.3}H_6$, Figs. 3d and 2e) with a structure of $Im\bar{3}m$-Y_3H_{18} where approximately every two out of three yttrium atoms are replaced by lanthanum. At the center of DAC M2_S, at 180 GPa we also detected a tetragonal phase impurity similar to previously detected *I*4/*mmm*-YH_4 [13], but with a unit cell volume larger by 1.4 Å^3/f.u. at this pressure. This enables us to assign this compound the composition La_2YH_{12} (Fig. 3e). The significant difference between the results of syntheses in DACs M1–2, SL1, SL3, and M2_S is probably due to the lack of hydrogen in DAC M2_S, which is indicated by the presence of impurities of lower tetrahydrides (Fig. 3).

Superconductivity

The superconducting properties of the obtained lanthanum–yttrium hydrides were studied by measuring the temperature dependence of the electrical resistance of the samples in various current modes using the four-probe method, with and without an external magnetic field (Fig. 4). The $Fm\bar{3}m$-(La,Y)H_{10} polyhydrides, synthesized from La_2Y and La_4Y, have similar properties and exhibit relatively wide (15–17 K) superconducting transition with T_C = 245–253 K at 183–199 GPa, with the resistance drop to 0.1 mΩ (Fig. 4a,b). In several DACs we detected an additional shelf in the $R(T)$ dependence at ~ 237 ± 5 K, possibly due to the presence of $Im\bar{3}m$-(La,Y)H_6 formed with less hydrogen. The admixture of YH_6, which forms sometimes, corresponds to the superconducting transition at 224–226 K (Supporting Information Figs. S27 and S29).

We investigated the pressure dependence of T_C for the (La,Y)H_{10} samples obtained from La_2Y, La_3Y, and La_4Y alloys (Supporting Information Figs. S28 and S30). For the first sample (La_2Y), when pressure in the DAC decreased from 196 to 183 GPa, the critical temperature of the corresponding superhydride increased from 244.5 K to 253 K with a gradient dT_C/dP = –0.65 K/GPa,

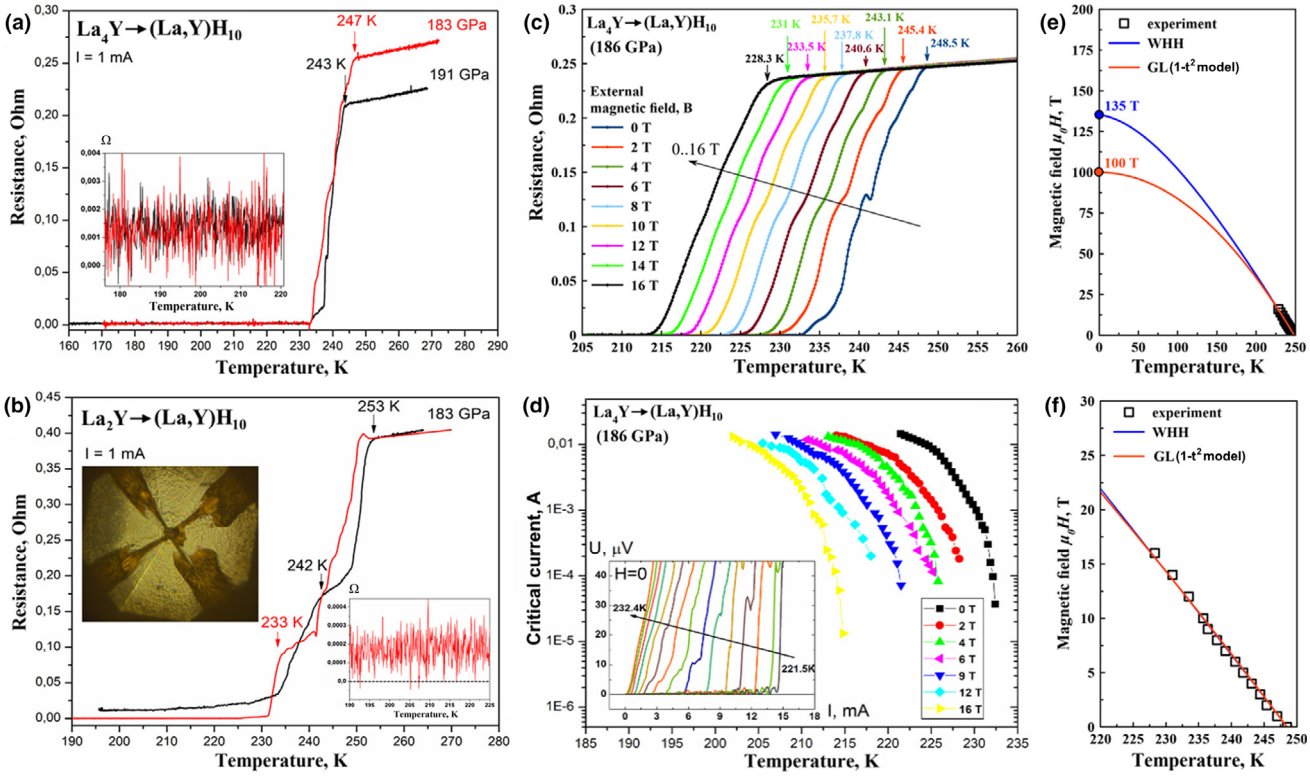

FIGURE 4

Superconducting transitions in $Fm\bar{3}m$-(La,Y)H_{10}: (a) Temperature dependence of the electrical resistance for the sample obtained from La_4Y. Inset: residual resistance after cooling below T_C. (b) Temperature dependence of the resistance for the sample obtained from La_2Y. Insets: residual resistance after cooling below T_C and a photo of the DAC culet with electrodes. (c) Dependence of the electrical resistance of (La,Y)H_{10} on the external magnetic field (0–16 T) at 186 GPa and 0.1 mA current. The critical temperatures were determined at the onset of the resistance drop. (d) Dependence of the critical current on the temperature and external magnetic field (0–16 T). The critical currents were measured near T_C. Inset: current–voltage characteristic near a superconducting transition. (e) Extrapolation of the upper critical magnetic field using the Werthamer–Helfand–Hohenberg theory [45] (WHH) and Ginzburg–Landau theory [46] (GL). (f) Dependence of the critical temperature T_C on the applied magnetic field.

whereas for La_4Y, the measured gradient was –0.13 K/GPa (Supporting Information Fig. S28a). The observed increase in the critical temperature is probably due to the near loss of dynamical stability of the $Fm\bar{3}m$-LaH_{10} structure and increase of the electron–phonon coupling (EPC) coefficient. The opposite situation was observed for La_3Y: with an increase in pressure from 157 to 181 GPa, the critical temperature grew very slowly from 243 to ~ 245 K with a slope $dT_C/dP = +0.071$ K/GPa (Supporting Information Fig. S30). Thus, the use of La_2Y alloy yielded the most efficient $(La,Y)H_{10}$ superconductor.

Measurements in external magnetic fields of 0–16 T (Fig. 4c, d, Supporting Information Figs. S27–S28) showed an almost linear $T_C(B)$ dependence with the slope $dB_{c2}/dT \approx -0.76$ T/K near 230–250 K (Fig. 4f). The extrapolated upper critical magnetic field $\mu_0H_{c2}(0)$ is 90–135 T, which is lower than that of YH_6, even though T_C, of $(La,Y)H_{10}$ is notably higher (see Supporting Information) than those of YH_6. This additionally indicates a possible anomaly in the mechanism of superconductivity in $Im\bar{3}m$-YH_6 [13]. In all the studied cases the upper critical magnetic field demonstrated a linear dependence $B_{c2}(T) \sim |T\text{-}T_C|$.

Going from binary to ternary hydrides, especially with similar atoms like La and Y, the possibility of structural disorder appears. The degree of disorder in such a system is expected to be much higher than in binary hydrides. The expected result of fluctuations in the composition will broaden the superconducting transitions in ternary and quaternary hydrides in comparison with binary ones, which is observed in Fig. 4b,c and Supporting Information Fig. S30. We think that this phenomenon will be a serious complicating factor in future studies of superconductivity in complex hydrides. It is possible to reduce the width of superconducting transitions by using a sort of "hardening"—increasing the time and number of laser heating and cooling cyclesduring which the quality of the resulting structure may be consistently improved.

One of the distinguishing features of superconductors is the existence of an upper limit of current density J_C at which superconductivity disappears and the material acquires nonzero electrical resistance. The critical currents and voltage–current (U–I) characteristics for the $(La,Y)H_{10}$ sample obtained from La_4Y alloy were investigated in the range from 10^{-5} to 10^{-2} A in external magnetic fields at 186 GPa (Fig. 4d). The critical current density was estimated on the basis of the facts that the sample size cannot exceed the size of the culet (50 μm) and the thickness of the sample is smaller than that of the gasket before the cell is loaded (~10 μm). This approach shows that the critical current density in $(La,Y)H_{10}$ is over 2 A/mm^2 at 230 K. More accurate measurements of the original La–Y samples using using the interference of light between diamond anvils (see Supporting Information Fig. S17) show that the thickness of the loaded metal particles does not exceed 1–1.5 μm. Taking into account the diameter of the samples (≈ 30 μm), we can refine the estimate for the critical current density as minimum 22 A/mm^2 at 230 K.

The analysis of the pinning force ($F_p = B \cdot I_C$) dependence on the magnetic field (Supporting Information Fig. S29a) shows that according to Dew-Hughes [47] the pinning in $(La,Y)H_{10}$ in the first approximation can be described as "dl-pinning". This allows us to extrapolate the $I_C(T)$ data to low temperatures within the single vortex model $J_C = J_{C0}(1 - T/T_C)^{5/2}(1 + T/T_C)^{-1/2}$. The extrapolation shows that at 4.2 K, the critical current I_C in the sample may reach 6 A and the critical current density J_C may exceed 12 kA/mm^2. The extrapolation using Ginzburg–Landau model [46] ($J_C = J_{C0}(1 - T/T_C)^{3/2}$) gives lower values at 4.2 K: the extrapolated critical current I_C in the sample can reach 1.25 A and the extrapolated critical current density J_{C0} at 0 K exceeding 2500 A/mm^2. These values are comparable with the parameters of NbTi and YBCO [48], and slightly higher than those in recently studied $Im\bar{3}m$-YH_6 [13]. Taking into account the more accurate SEM and optical measurements of the sample sizes, we can refine the estimate for J_C as minimum 27.7 kA/mm^2 at 4.2 K (GL-model).

The first-principles analysis of the superconducting properties of the La–Y–H phases was performed within the harmonic approximation for phonons. We calculated parameters of the electron–phonon coupling and the superconducting state for a series of hexahydrides ($Im\bar{3}m$-LaH_6, cubic La_4YH_{30}, La_2YH_{18}, $Pm\bar{3}m$-$LaYH_{12}$) and for a decahydride pseudocubic $R\bar{3}m$-$LaYH_{20}$ (obtained from $Fm\bar{3}m$-La_2H_{20} by the La→Y replacement) at 180 GPa using the tetrahedron method of integration over the Brillouin zone [49] (Table 2, Supporting Information Tables S7–S8). To simplify the analysis, here we discuss in detail only the results of the calculations for high-symmetry decahydride $R\bar{3}m$-$LaYH_{20}$ with a regular arrangement of the lanthanum and yttrium atoms.

At 180 GPa, the EPC coefficient λ of $Pm\bar{3}m$-$LaYH_{12}$ reaches 2.82, ω_{log} is 847 K, and the critical temperature T_C calculated using the Migdal–Eliashberg approach [50,52] is 223–241 K within the common range of the Coulomb pseudopotential $\mu^* = 0.15$–0.1. A decrease in the concentration of yttrium in $(La,Y)H_6$ leads to an increase in T_C of La_2YH_{18} and La_4YH_{30} to 265–270 K ($\mu^* = 0.1$). Keeping in mind that the H sublattice in $(La,Y)H_6$ has almost the same structure as in YH_6, we can expect a negative anharmonic contribution $\Delta T_C \sim 25$–30 K, as in pure yttrium hexahydride [13]. These estimates are in good agreement with the experimentally observed critical temperature of 237 ± 5 K. Calculations within the Migdal–Eliashberg (ME) theory show that the expected upper critical magnetic field $\mu_0H_{C2}(0)$

TABLE 2

Parameters of the superconducting state of $R\bar{3}m$-LaYH$_{20}$, $Pm\bar{3}m$-LaYH$_{12}$, and $Im\bar{3}m$-LaH$_6$ at 180 GPa calculated using the isotropic Migdal–Eliashberg equations (E) [50] and the Allen–Dynes formula (AD) [51] with $\mu^* = 0.15$–0.1.

Parameter	$R\bar{3}m$-LaYH$_{20}$	$Pm\bar{3}m$-LaYH$_{12}$	$Im\bar{3}m$-LaH$_6$
λ	3.87	2.82	2.41
ω_{log}, K	868	847	1011
T_C (AD), K	232–266	176–203	180–207
T_C (E), K	281–300*	223–241	217–235
T_C (SCDFT), K	252	191	176
$N(E_F)$, states/eV/metal atom	0.87	0.8	1.62
Δ(0), meV	67–71	53–57.5	49–54
$\mu_0H_{C2}(0)$, T	99–101	73–77	98–106
$R_\Delta = 2\Delta(0)/k_BT_C$	5.48–5.54	5.5	5.23–5.35

*T_C (E) = 266 K at $\mu^* = 0.2$.

of $(La,Y)H_6$ is ~ 70–80 T and the superconducting gap is around 60 meV (Table 2, Supporting Information Table S8). We believe that the enhanced superconducting properties of $(La,Y)H_6$ compared to pure YH_6 are related to the presence of distorted $Im\bar{3}m$-LaH_6 in the crystal structure, which results in an increase in the electron–phonon interaction coefficient from 2.24 in YH_6 (harmonic approach [13]) to 2.41–2.82 in $(La,Y)H_6$.

Our calculations within Migdal–Eliashberg (ME) [50,52] theory show that decahydride $R\bar{3}m$-$LaYH_{20}$ has the EPC coefficient of 3.87 and ω_{log} = 868 K, which are comparable to the parameters of LaH_{10} [53], and result in theoretical T_C^{ME} = 281–300 K within the common range of the Coulomb pseudopotential μ^* = 0.15–0.1. Because the structure of $R\bar{3}m$-$LaYH_{20}$ is similar to that of LaH_{10}, we can expect the negative anharmonic contribution ΔT_C of ~ 25–35 K [34] to reduce T_C to about 265 K. Calculations within Migdal–Eliashberg theory show that for $(La,Y)H_{10}$ the expected upper critical magnetic field $\mu_0 H_{C2}(0)$ is 100 T, the superconducting gap is around 70 meV, and the coherence length $\xi_{BCS} = 0.5\sqrt{h/\pi e H_{C2}}$ is close to 16 Å (Supporting Information Table S8). In contrast to the $Im\bar{3}m$-XH_6 (X = La, Y) structures, the calculations within density functional theory for superconductors (SCDFT) yield T_C = 252 K for $R\bar{3}m$-$LaYH_{20}$ at 180 GPa, which is close to both the ME theory and experimental results. Experimentally found T_C = 253 K and extrapolated $\mu_0 H_{C2}(0)$ = 100–135 T of $(La,Y)H_{10}$ are in close agreement with the theoretically calculated values, which means that superconductivity in the La–Y–H ternary decahydrides is described well in the framework of the classical Bardeen–Cooper–Schrieffer [54,55] and Migdal–Eliashberg theories.

Conclusions

Ternary hydrides represent the most promising direction for studies of superconductivity under pressure. The primary objective in this field is to achieve room-temperature transition at the lowest possible pressure. Such superconductors, synthesized in miniature (d_{out} ~ 10–15 mm) high-pressure anvil cells, may find multiple applications in microelectronics. In fact, diamond anvil culet provides enough space (20x20μm) for creating relatively complex optical and magnetic sensors using lithographic methods.

In this work, novel high-T_C ternary superconducting hydrides $Im\bar{3}m$-$(La,Y)H_6$ and $Fm\bar{3}m$-$(La,Y)H_{10}$ were experimentally discovered together with $I4/mmm$-$(La,Y)H_4$ at pressures of 170–196 GPa. Using the La – Y alloys (with 1:1, 2:1, 3:1, 4:1, and 1:4 ratios) as a precursor for high-pressure synthesis, we replaced about 25% of lanthanum atoms in the structure of LaH_{10} with yttrium. Moreover, we found that about 70% of the yttrium atoms in YH_6 can be replaced by La without decomposition of the $Im\bar{3}m$ sodalite-like structure of the hexahydride. In other words, superhydrides that do not exist at 180 GPa can nevertheless be stabilized as a solid solution: $Y@H_{32}$ cages with the local H environment specific for $Fm\bar{3}m$-YH_{10} can exist in the $Fm\bar{3}m$-LaH_{10} environment, whereas $Im\bar{3}m$-LaH_6 can be stabilized by introducing only 30% of yttrium.

At 183 GPa, the obtained $Fm\bar{3}m$-$(La,Y)H_{10}$ decahydrides demonstrate outstanding T_C of up to 253 K, the superconducting gap of ~ 70 meV, and the extrapolated upper critical magnetic field of 100–135 T in close agreement with the calculations within ME theory. The estimated critical current density (12–27.7 kA/mm^2) at 4.2 K in lanthanum–yttrium decahydride may exceed that of YBCO, NbTi, and YH_6.

We believe the performed experiments will have a strong impact on subsequent studies of ternary metal–hydrogen systems, opening promising ways to stabilize such exotic compounds as MgH_6 [56,57], ZrH_{10} [58,59], CaH_6 [60], PdH_2 [61], PdH_{10} [62], and others which cannot be obtained by direct synthesis but may exist in the form of a solid solution with known superhydrides at relatively low pressures.

Methods

Experiment

To perform the X-ray diffraction study, seven diamond anvil cells (DACs M1, M2, M2_S, SL1, SL1_S, SL3, and SL3_S) were loaded. The diameter of the working surface of the diamond anvils was 280 μm beveled at an angle of 8.5° to a culet of 50 μm. Composite gaskets consisting of a tungsten ring and a CaF_2/epoxy mixture were used to isolate the electrical leads. Lanthanum–yttrium pieces with a thickness of ~ 1–2 μm were sandwiched between the electrodes and ammonia borane NH_3BH_3 (AB) in the gasket hole with a diameter of 20 μm and a thickness of 10–12 μm. Laser heating of samples above 2000 K at pressures of 170–196 GPa by a series of laser pulses with a duration of 100–400 milliseconds led to the formation of ternary lanthanum–yttrium hydrides the structure of which was analyzed using X-ray diffraction. Because each laser heating and cooling cycle resulted in some pressure change in the DACs, the pressure in each experiment was determined separately. Raman and X-ray diffraction studies showed the absence of byproducts of the AB thermal decomposition in the obtained hydrides.

X-ray diffraction patterns of the samples in DACs M1-2, SL1, and SL3 were recorded at the ID15B synchrotron beamline at the European Synchrotron Radiation Facility (Grenoble, France) using a focused (5 × 5 μm) monochromatic X-ray beam with a wavelength of 0.4111 Å and Mar555 detector. The exposure time was 60 s. CeO_2 standard was used for the distance calibration. The X-ray diffraction data were analyzed and integrated using Dioptas software package (version 0.5) [63]. The full profile analysis of the diffraction patterns and the calculation of the unit cell parameters were performed in JANA2006 program [64] using the Le Bail method [65]. The pressure in the DACs was determined via the Raman signal of diamond [66].

X-ray diffraction patterns of the $La_xY_{1-x}H_6$ sample (DAC M2_S) were recorded at the BL10XU beamline (SPring-8, Japan) using monochromatic synchrotron radiation and an imaging plate detector at room temperature [67,68]. The X-ray beam with a wavelength of 0.413 Å was focused in a 3 × 8 μm spot with a polymer refractive lens (SU-8, produced by ANKA).

Powder XRD experiments with DACs SL1_S and SL3_S were carried out at beamline P02.2 of PETRA III, DESY (Hamburg) [69]. The X-ray wavelength was λ = 0.2906 Å, and the beam size was 2 × 2 μm at full width at half maximum (FWHM). The calibration was performed using CeO_2 standard. For data collection, a fast flat panel detector XRD1621 from Perkin Elmer (2048 pix-

els × 2048 pixels with 200 × 200 μm pixel size) was used. All (La,Y)H_x samples were mapped using a 10 × 10 or 12 × 12 grid with a step of 2 μm, and XRD was examined for each point of this map.

The initial La–Y alloys used as the precursors for the high-pressure synthesis of ternary hydrides were fused and then characterized using XRD, energy-dispersive X-ray fluorescence (EDXRF) analysis, and scanning/transmission electron microscopy (SEM/TEM). To prepare La_2Y alloy, pure metals La and Y (99.9%, CHEMCRAFT Ltd.) were crushed, washed in dilute HCl and acetone to remove impurities, and dried in a glove box. The components were weighed and mixed in a specified ratio. Heating was carried out resistively. The melt was kept in tantalum crucibles at a temperature of 1900 K in an inert atmosphere (helium) for one hour and quenched at an initial rate of 200 K/min.

XRD patterns of the La–Y alloys were recorded using the powder X-ray diffractometer Rigaku MiniFlex 600 (Rigaku, Japan) with CuK_α radiation (40 kV, 15 mA, Ni–K_β-filter) in the 2θ angle range from 20° to 115° with a scanning step of 0.02° and a rate of 0.7°/min. The phases were identified in the PXDRL program (Rigaku, Japan) using ICDD PDF-2 datasets (release 2017). The unit cell parameters were refined in JANA2006 program [64] using Le Bail method [65]. The elemental analysis of the initial La–Y alloys was performed using the energy-dispersive EDXRF in μ-XRF system ORBIS PC (EDAX, USA). The EDXRF spectra were collected under vacuum from 2 mm areas of the samples irradiated using Rh X-ray tube at 30 kV and 100 μA during 30 s.

The morphology and composition of the initial LaY alloy used as a precursor for La_2YH_x hydride (DAC M2_S) were studied using the scanning electron microscope (SEM) Scios (ThermoFisher Scientific, USA) equipped with an energy-dispersive X-ray (EDX) spectrometer and an Octane Elite silicon drift detector (SDD) with Si_3N_4 window (EDAX, USA). The acceleration voltage was 30 kV. For the SEM and EDX studies, the chunk of the alloy was polished on one side using diamond powder with sequentially reduced particle sizes. The specimen for scanning/transmission electron microscopy (S/TEM) was prepared in the focused ion beam (FIB) scanning electron microscope Scios (ThermoFisher Scientific, USA) by a standard lift-out FIB technique at an accelerating voltage of Ga^+ ions of 30 kV at the initial and 5 kV at the final step. Microstructural and elemental analyses were performed in an Osiris TEM/STEM (ThermoFisher Scientific, USA) equipped with the EDX Super-X SDD spectrometer (Bruker, USA), the high-angle annular dark field (HAADF) electron detector (Fischione, USA) and a 2048 × 2018 Gatan CCD (Gatan, USA). Image processing was performed using Digital Micrograph (Gatan, USA) and TIA (ThermoFisher Scientific, USA) software. Simulations of the ED patterns and images were produced using Stadelmann's EMS software package [70].

Magnetotransport measurements were performed on samples with at least two hydride phases, therefore the voltage contacts in the Van der Pauw method might have been connected to a low-T_C phase. As a result, the superconducting transition in the main phase $(La,Y)H_{10}$ can be observed as an upward feature of the resistance–temperature curves because of the shunting effect in fine-grained samples.

In Fig. S29, the plot of the normalized volume pinning force F_p/F_p^{max} versus the reduced field $h = H/H_{c2}$ is drawn on the basis of interpolation of the $J_C(T, B)$ data. The experimental data were fitted using the Dew-Hughes (DH) model [47] for surface type normal pinning centers $f \sim h^p(1-h)^q$. For this model, the parameters are: $p = 0.5$, $q = 2$, $h_{max} = 0.2$, which is close to our fit. Depinning critical current for this type of pinning can be described within the model of single vortices, where vortices are pinned on randomly distributed weak pinning centers via spatial fluctuations of the charge carrier mean free path, or, in other words, "dl-pinning".

Theory

Computational predictions of thermodynamic stability of the La–Y–H phases at 200 GPa were carried out using the variable-composition evolutionary algorithm USPEX [27,71,72]. The first generation consisting of 120 structures was produced using the random symmetric [72] and random topological [73] generators, whereas all subsequent generations contained 20% of random structures and 80% of those created using heredity, softmutation, and transmutation operators. The evolutionary searches were combined with structure relaxations using density functional theory (DFT) [74,75] within the Perdew–Burke–Ernzerhof functional (generalized gradient approximation) [42] and the projector augmented wave method [39,76] as implemented in the VASP code [36,38,77]. The kinetic energy cutoff for plane waves was 600 eV. The Brillouin zone was sampled using Γ-centered k-points meshes with a resolution of $2\pi \times 0.05$ Å^{-1}. This methodology is similar the one used in our previous works [78,79].

The same techniques and parameters as those used for structure relaxations were implemented to calculate the equations of state. We also calculated the phonon densities of states of the studied materials using the finite displacements method (VASP and PHONOPY [80,81]).

The calculations of the critical temperature of superconductivity T_C were carried out using Quantum ESPRESSO (QE) package [40,41]. The phonon frequencies and electron–phonon coupling (EPC) coefficients were computed using density functional perturbation theory [82], employing the plane-wave pseudopotential method and Perdew–Burke–Ernzerhof exchange–correlation functional [42]. In our ab initio calculations of the electron–phonon coupling (EPC) coefficient λ, the first Brillouin zone was sampled using a 3 × 3 × 3 or 4 × 4 × 4 q-points mesh and a denser 16 × 16 × 16 k-points mesh for the La–Y–H phases. T_C was calculated by solving Eliashberg equations [50] using the iterative self-consistent method for the imaginary part of the order parameter $\Delta(T, \omega)$ (superconducting gap) and the renormalization wave function $Z(T, \omega)$ [83]. More approximate estimates of T_C were made using the Allen–Dynes formula [51].

Finally, we also solved the gap equation in density functional theory for superconductors (SCDFT) [84,85] for evaluating T_C of $Im\bar{3}m$-LaH_6, $LaYH_{12}$, and $R\bar{3}m$-$LaYH_{20}$ nonempirically:

$$\Delta_{nk}(T) = -Z_{nk}(T)\Delta_{nk}(T) - \frac{1}{2}\sum_{n'k'} K_{nkn'k'}(T)\frac{\tanh \beta E_{n'k'}}{E_{n'k'}}\Delta_{n'k'}(T), \qquad (1)$$

where $E_{n'k'} = \sqrt{\xi^2_{n'k'} + \Delta^2_{n'k'}}$. The temperature (as $\beta = 1/T$) dependence of the order parameter Δ_{nk} indicates T_C. Labels n, n', k, and k' denote the Kohn–Sham band and momentum indices,

respectively. ξ_{nk} is the energy eigenvalue of state nk measured from the Fermi level, as calculated using the standard Kohn–Sham equation for the normal state. $Z_{nk}(T)$ and $K_{nkn'k'}(T)$ represent the electron–phonon and electron–electron Coulomb interaction effects, the formulas for which have been constructed so that the self-energy corrections, almost the same as those in the Eliashberg equations with the Migdal approximation [50,52,86,87], are included (see Supplemental materials of Kruglov et al. [53] for details, which is based on Refs. [84,85,88,89]). We calculated the screened electron–electron Coulomb interaction within the random phase approximation [90], electronic density of states (DOS) of the normal state was used for solving eq (1). We generated dense ξ_{nk} data points entering eq (1) around E_F by a linear interpolation from the values on a dense k-point mesh.

Author contributions

I.A.T, D.V.S., M.H., K.V.G., N.G., A.G.I., and A.G.K. performed the experiments. I.A.T., A.V.S., and O.A.S. performed the superconductivity measurements. D.V.S., A.G.K., R.A., and A.R.O. prepared the theoretical analysis. D.V.S., A.G.K., and A.G.I. contributed to the interpretation of the results. D.V.S., A.G.K., and A.R.O. wrote the manuscript. A.V.S., O.A.S., and V.M.P. performed the magnetotransport experiments in high magnetic fields and participated in the data processing and discussions. D.N.K., A.L.V., and K.S.P. prepared the La–Y alloys. R.A. performed the SCDFT calculations. I.S.L. directed the research and edited the manuscript. I.A.K. performed the T-USPEX and anharmonic phonon density of states calculations. All the authors provided critical feedback and helped shape the research, analysis, and manuscript.

Declaration of Competing Interest

The authors declare that they have no known competing financial interests or personal relationships that could have appeared to influence the work reported in this paper.

Acknowledgments

The work was performed on the ESRF (Grenoble, France) station ID15B, on SPring-8 (Sayo, Japan) station BL10XU (project No. 2019B1476), and at P02.2 station of PETRA III, DESY (Hamburg, Germany). The high-pressure experiments were supported by the Ministry of Science and Higher Education of the Russian Federation within the state assignment of the FSRC Crystallography and Photonics of RAS and by the Russian Science Foundation (Project No. 19-12-00414). A.G.K. thanks Russian Foundation for Basic Research, project 19-03-00100, for the financial support of this work. A.R.O. thanks Russian Science Foundation (grant 19-72-30043). D.V.S. thanks the Russian Foundation for Basic Research (project 20-32-90099). The authors express their gratitude to the staff of the station BL10XU of SPring-8 synchrotron research facility, especially to Dr. Saori Kawaguchi (JASRI), for the tremendous assistance in the use of the station's equipment before and after the experiment. SEM, TEM, XRF and XRD studies of the initial alloys were performed using the equipment of the Shared Research Center FSRC "Crystallography and photonics" RAS. I.A.T. and A.G.I. acknowledge the use of the facilities of the Center for Collective Use "Accelerator Center for Neutron Research of the Structure of Substance and Nuclear Medicine" of the INR RAS for high-pressure cell preparation. I. A.T. and A.G.I. thank Viktor Struzhkin and the Center for High Pressure Science and Technology Advanced Research (HPSTAR, China) for support in the experiments at SPring-8. The research used resources of the LPI Shared Facility Center. A.V.S., O.A.S. acknowledge the support of the state assignment of the Ministry of Science and Higher Education of the Russian Federation (Project No. 0023-2019-0005). V.M.P. thanks the Russian Foundation for Basic Research (project 21-52-12043). K.S.P. thanks the Russian Foundation for Basic Research (project 19-02-00888). This work was supported by JSPS KAKENHI Grant Number 20K20895. Some calculations were performed at the Supercomputer Center at the Institute for Solid State Physics in the University of Tokyo. I.A.K. thanks the Russian Science Foundation (grant No. 19-73-00237) for the financial support of the development of T-USPEX method and anharmonic phonon density of states calculations algorithm. We also thank Igor Grishin (Skoltech) for proofreading the manuscript, and Ilya Krupatin (Skoltech) for help with Helios G4 Plasma FIB Uxe. Access to the Scanning Electron Microscopy (SEM) facilities was granted by the Advanced Imaging Core Facility (AICF) of Skoltech.

Data availability

The raw and processed data required to reproduce these findings are available to download as Supporting Information for the manuscript.

Appendix A. Supplementary data

Supplementary data to this article can be found online at https://doi.org/10.1016/j.mattod.2021.03.025.

References

[1] N.W. Ashcroft, Phys. Rev. Lett. 92 (2004) 187002.
[2] P. Cudazzo et al., Phys. Rev. B 81 (2010) 134505.
[3] P. Cudazzo et al., Phys. Rev. B 81 (2010) 134506.
[4] R.P. Dias, I.F. Silvera, Science 355 (2017) 715–718.
[5] J.M. McMahon et al., Rev. Mod. Phys. 84 (2012) 1607–1653.
[6] S. Azadi et al., Phys. Rev. Lett. 112 (2014) 165501.
[7] J. McMinis et al., Phys. Rev. Lett. 114 (2015) 105305.
[8] A.P. Drozdov et al., Nature 525 (2015) 73–76.
[9] M. Somayazulu et al., Phys. Rev. Lett. 122 (2019) 027001.
[10] A.P. Drozdov et al., Nature 569 (2019) 528.
[11] E. Snider et al., Nature 586 (2020) 373–377.
[12] Z.M. Geballe et al., Angew. Chem. Int. Ed. 57 (2017) 688–692.
[13] I. Troyan et al., Adv. Mater. (2021) e2006832.
[14] P.P. Kong, et al., ArXiv:1909.10482 [Cond-Mat] (2019).
[15] L.Y. Fang, Chin. Phys. Lett. 37 (2020) 107401
[16] E. Snider et al., Phys. Rev. Lett. 126 (2021) 117003.
[17] Y. Li et al., Sci. Rep. 5 (2015) 09948.
[18] H. Liu et al., PNAS 114 (2017) 6990–6995.
[19] X. Liang et al., Phys. Rev. B 99 (2019) 100505.
[20] W. Sukmas et al., J. Alloys Compounds 849 (2020) 156434.
[21] Y. Sun et al., Phys. Rev. Lett. 123 (2019) 097001.
[22] D. Zhou, et al., in: Book of Abstracts of AIRAPT 27, Rio de Janeiro, 2019.
[23] M. Kostrzewa et al., Sci. Rep. 10 (2020) 1–8.
[24] C. Heil et al., Phys. Rev. B 99 (2019) 220502.
[25] C.W. Glass, A.R. Oganov, N. Hansen, Comput. Phys. Commun. 175 (2006) 713–720.
[26] A.R. Oganov et al., Rev. Mineral Geochem. (2010) 271–298.
[27] A.R. Oganov, A.O. Lyakhov, M. Valle, Acc. Chem. Res. 44 (2011) 227–237.
[28] P. Song, et al. ArXiv:2103.06690 [Cond-Mat, Physics:Physics] (2021).
[29] D. Zhou et al., Sci. Adv. 6 (2020) eaax6849.
[30] D. Zhou et al., J. Am. Chem. Soc. 142 (2020) 2803–2811.

[31] D.V. Semenok et al., J. Phys. Chem. Lett. (2020) 32–40.
[32] D.V. Semenok et al., Mat. Today 33 (2020) 36–44.
[33] W. Chen et al., Nat. Comm. 12 (2021) 273.
[34] I. Errea et al., Nature 578 (2020) 66–69.
[35] D. Sun, et al., ArXiv:2010.00160 [Cond-Mat] (2020).
[36] G. Kresse, J. Hafner, Phys. Rev. B 47 (1993) 558–561.
[37] G. Kresse, J. Furthmüller, Comp. Mat. Sci. 6 (1996) 15–50.
[38] G. Kresse, J. Furthmüller, Phys. Rev. B 54 (1996) 11169–11186.
[39] G. Kresse, D. Joubert, Phys. Rev. B 59 (1999) 1758–1775.
[40] P. Giannozzi et al., J. Phys.: Condense. Matter 21 (2009) 395502.
[41] P. Giannozzi et al., J. Phys.: Condens. Matter 29 (2017) 465901.
[42] J.P. Perdew, K. Burke, M. Ernzerhof, Physical Review Letters 77 (1996) 3865–3868.
[43] F. Birch, Phys. Rev. 71 (1947) 809–824.
[44] F.D. Murnaghan, Proc. Natl. Acad. Sci. U S A 30 (1944) 244–247.
[45] N.R. Werthamer, E. Helfand, P.C. Hohenberg, Phys. Rev. 147 (1966) 295–302.
[46] V.L. Ginzburg, L.D. Landau, Zh. Eksp Teor. Fiz. 20 (1950) 1064–1082.
[47] D. Dew-Hughes, Philos. Mag. 30 (1974) 293–305.
[48] J. Schwartz, et al., ArXiv:1108.1634 [Physics] (2011).
[49] M. Kawamura, Y. Gohda, S. Tsuneyuki, Phys. Rev. B 89 (2014) 094515.
[50] G.M. Eliashberg, JETP 11 (1959) 696–702.
[51] P.B. Allen, R.C. Dynes, Phys. Rev. B 12 (1975) 905–922.
[52] A.B. Migdal, JETP 34 (1958) 996–1001.
[53] I.A. Kruglov et al., Phys. Rev. B 101 (2020) 024508.
[54] J. Bardeen, L.N. Cooper, J.R. Schrieffer, Phys. Rev. 106 (1957) 162–164.
[55] J. Bardeen, L.N. Cooper, J.R. Schrieffer, Phys. Rev. 108 (1957) 1175–1204.
[56] X. Feng et al., RSC Adv. 5 (2015) 59292–59296.
[57] R. Szczęśniak, A.P. Durajski, Front. Phys. 11 (2016) 117406.
[58] H. Xie et al., J. Phys. Chem. Lett. 11 (2020) 646–651.
[59] K. Abe, Phys. Rev. B 98 (2018) 134103.
[60] H. Wang et al., PNAS 109 (2012) 6463–6466.
[61] Z. Liu et al., Sci. Rep. 10 (2020) 8037.
[62] P.-W. Guan, R.J. Hemley, V. Viswanathan, ArXiv:2007.15613 [Cond-Mat, Physics:Physics] (2020).
[63] C. Prescher, V.B. Prakapenka, High Pressure Research 35 (2015) 223–230.
[64] V. Petříček, M. Dušek, L. Palatinus, Zeitschrift Für Kristallographie - Crystalline Materials 229 (2014) 345–352.
[65] A.L. Bail, Powder Diffraction 20 (2005) 316–326.
[66] M.I. Eremets, J. Raman Spectrosc. 34 (2003) 515–518.
[67] Y. Ohishi et al., High Pressure Res. 28 (2008) 163–173.
[68] N. Hirao et al., Matter Radiation Extremes 5 (2020) 018403.
[69] H.-P. Liermann et al., J. Synchrotron. Rad. 22 (2015) 908–924.
[70] G. van Tendeloo, D. van Dyck, S.J. Pennycook, eds., Handbook of Nanoscopy, 2nd ed., Wiley, n.d.
[71] A.R. Oganov, C.W. Glass, J. Chem. Phys. 124 (2006) 244704.
[72] A.O. Lyakhov et al., Comput. Phys. Commun. 184 (2013) 1172–1182.
[73] P.V. Bushlanov, V.A. Blatov, A.R. Oganov, Comput. Phys. Commun. 236 (2019) 1–7.
[74] P. Hohenberg, W. Kohn, Phys. Rev. 136 (1964) B864–B871.
[75] W. Kohn, L.J. Sham, Phys. Rev. 140 (1965) A1133–A1138.
[76] P.E. Blöchl, Phys. Rev. B 50 (1994) 17953–17979.
[77] G. Kresse, J. Hafner, Phys. Rev. B 49 (1994) 14251–14269.
[78] D.V. Semenok et al., J. Phys. Chem. Lett. 9 (2018) 1920–1926.
[79] A.G. Kvashnin et al., ACS Appl. Mater. Interfaces 10 (2018) 43809–43816.
[80] A. Togo, I. Tanaka, Scripta Mater. 108 (2015) 1–5.
[81] A. Togo, F. Oba, I. Tanaka, Phys. Rev. B 78 (2008) 134106.
[82] S. Baroni et al., Rev. Modern Phys. 73 (2001) 515–562.
[83] P.B. Allen, R.C. Dynes, Technical Report #7 TCM/4/1974 (1974).
[84] M. Lüders et al., Phys. Rev. B 72 (2005) 024545.
[85] M.A.L. Marques et al., Phys. Rev. B 72 (2005) 024546.
[86] D.J. Scalapino, in: R.D. Parks (Ed.), Superconductivity: Part 1 (In Two Parts), Dekker, New York, 1969.
[87] J.R. Schrieffer, Theory of Superconductivity, 1 edition., Perseus Books, Reading, Mass, 1999.
[88] R. Akashi, R. Arita, Phys. Rev. B 88 (2013) 014514.
[89] R. Akashi et al., Phys. Rev. B 91 (2015) 224513.
[90] D. Pines, Elementary Excitations in Solids: Lectures on Phonons, Electrons, and Plasmons, Perseus, Reading, Mass, 1999.